Protein Engineering, Design & Selection vol. 27 no. 10 pp. 317–324, 2014
Published online August 4, 2014 doi:10.1093/protein/gzu030

Enhanced immunoPET of ALCAM-positive colorectal carcinoma using site-specific ^{64}Cu-DOTA conjugation

Richard Tavaré[1], Wei H.Wu[1], Kirstin A.Zettlitz[1], Felix B.Salazar[1], Katelyn E.McCabe[1], James D.Marks[2] and Anna M. Wu[1,3]

[1]Crump Institute for Molecular Imaging, Department of Molecular and Medical Pharmacology, David Geffen School of Medicine at UCLA, Los Angeles, CA 90095, USA and [2]Department of Anesthesia, UCSF, San Francisco General Hospital, San Francisco, CA 94110, USA

[3]To whom correspondence should be addressed. E-mail: awu@mednet.ucla.edu

Received July 2, 2014; revised July 2, 2014; accepted July 3, 2014

Edited by Dario Neri

Activated leukocyte cell adhesion molecule (ALCAM) is an immunoglobulin superfamily cell adhesion molecule that is aberrantly expressed in a wide variety of human tumors, including melanoma, prostate cancer, breast cancer, colorectal carcinoma, bladder cancer and pancreatic adenocarcinoma. This wide spectrum of human malignancies makes ALCAM a prospective pan-cancer immunoPET target to aid in detection and diagnosis in multiple malignancies. In this study, we assess site-specific versus non-site-specific conjugation strategies for ^{64}Cu-DOTA (1,4,7,10-tetraazacyclododecane-1,4,7,10-tetraacetic acid) immunoPET imaging of a fully human ALCAM cys-diabody (cDb) with a reduced linker length that retains its bivalent binding ability. ALCAM constructs with linker lengths of eight, five and three amino acids were produced to make true non-covalent site-specifically modified cDbs. Characterization by gel electrophoresis, size exclusion chromatography, flow cytometry and mass spectrometry of the various constructs was performed. To demonstrate the increased utility of targeting multiple malignancies expressing ALCAM, we compare the targeting of the site-specific versus non-site-specific conjugated cDbs to the human colorectal cancer xenograft LS174T. Interestingly, the conjugation strategy not only affects tumor targeting but also hepatic and renal uptake/clearance.

Keywords: ALCAM/Cu-64/DOTA/immunoPET/site-specific conjugation

Introduction

Activated leukocyte cell adhesion molecule (ALCAM/CD166) is a 110 kDa cell surface glycoprotein that forms homotypic adhesion as well as heterotypic adhesion with CD6 expressed on activated leukocytes (Bowen *et al.*, 1995; Patel *et al.*, 1995). Altered ALCAM expression has been found to be important on a wide variety of malignancies, including melanoma (van Kempen *et al.*, 2000; Swart *et al.*, 2005), pancreatic cancer (Chen *et al.*, 2005), prostate cancer (Kristiansen *et al.*, 2005), breast cancer (King *et al.*, 2004), ovarian cancer (Mezzanzanica *et al.*, 2008), acute myeloid leukemia (Strassberger *et al.*, 2014) and colorectal carcinoma (Weichert *et al.*, 2004). The exact role of upregulation or downregulation of ALCAM expression in tumorigenesis and metastatic potential of these malignancies is not completely understood (Ofori-Acquah and King, 2008). However, ALCAM detection as an accessible target for antibody targeting (Schliemann *et al.*, 2010) and the altered expression of ALCAM in multiple malignancies makes it a promising target for both detection (McCabe *et al.*, 2012) and therapy (Wiiger *et al.*, 2010). Recent findings demonstrating ALCAM expression on hematopoietic stem and progenitor cells might limit the use of ALCAM antibody-based therapy or require allogeneic stem cell transplantation post-therapy (Chitteti *et al.*, 2014; Strassberger *et al.*, 2014).

Immuno-positron emission tomography (immunoPET), whereby antibodies or their fragments are conjugated to PET radionuclides for subsequent PET acquisition, has generated considerable interest for the identification and quantification of tissue biomarkers *in vivo* (Wu and Senter, 2005; Wu, 2009). It is the high sensitivity and intrinsic quantification of PET coupled with the specificity and affinity of antibodies that make immunoPET an attractive translatable imaging modality for the detection of disease-specific biomarkers in the clinic (Knowles and Wu, 2012).

To obtain high target-to-background immunoPET images, the pharmacokinetic properties of the imaging agent, i.e. target tissue uptake and blood clearance, need to be optimized for the specific radionuclide used. Intact antibodies interact with the neonatal Fc receptors via the Fc portion of the antibody in a pH-dependent manner allowing for antibody recycling and persistent circulation of ~1–3 weeks. Copper-64 (^{64}Cu) has many applications for the development of radiopharmaceuticals for PET imaging (Anderson and Ferdani, 2009). However, it has a half-life of 12.7 h, making it unsuitable for the conjugation to intact antibodies and imaging past 2 days post-injection. Therefore, engineered antibody fragments that lack the full Fc domain, like the diabody (Db) and minibody (Mb) that have terminal serum half-lives of 2–5 and 5–12 h, respectively, are more compatible for ^{64}Cu-immunoPET (Wu, 2013).

Dbs (~50 kDa) are non-covalent single-chain variable fragment (scFv ~25 kDa) dimers that are constructed by reducing the linker length of an scFv between the V_H and V_L domains from 15–18 amino acids to 3–8 amino acids, forcing them to form interchain-V_H and V_L pairing resulting in bivalent Dbs and not intrachain-V_H and V_L pairing resulting in scFvs. Dbs exhibit increased tumor uptake due to their bivalent avidity and longer half-life compared with scFvs. Furthermore, cysteine residues can be engineered into the Db construct to produce covalent cysteine-modified diabodies, or cys-diabodies (cDbs) (Li *et al.*, 2002; Olafsen *et al.*, 2004). The engineered cysteine allows for the site-specific conjugation of thiol-reactive fluorophores (Sirk *et al.*, 2008), quantum dots (Barat *et al.*, 2009) or bifunctional chelators (Olafsen *et al.*, 2004). As opposed to non-site-specific conjugation, site-specific conjugation allows for a single, uniform product instead of a distribution of

conjugations to the protein of interest. Species with the greater number of conjugates using non-site-specific conjugations to radiometal chelators are likely less functional due to modification at the binding site of the antibody. Furthermore, these more highly-conjugated species are likely to carry more radioactivity, which when used for imaging purposes will result in most of the radioactive signal originating from inactive/non-functional radiolabeled protein. The importance of site specificity has been proven in many systems, including antibody–drug conjugation (Junutula *et al.*, 2008), protein immobilization (Camarero, 2008) and molecular imaging (Tait *et al.*, 2006; Tavaré *et al.*, 2009), among others, due to defined, reproducible conjugations and directing the modification away from the active or binding site of the protein undergoing conjugation. Furthermore, groups have examined many other ways, including unnatural amino acids and click chemistry, to incorporate bio-orthogonal site-specific conjugations for protein modification (Sletten and Bertozzi, 2009; Liu and Schultz, 2010).

Recently, a cross-reactive human and mouse anti-ALCAM scFv was derived from an internalizing human scFv phage library (Liu *et al.*, 2004; Liu *et al.*, 2007). After reformatting into a diabody by reducing the linker length from 15 to 8 amino acids, it was conjugated to the chelator 1,4,7,10-tetraazacyclododecane-1,4,7,10-tetraacetic acid (DOTA) using a non-site-specific approach for subsequent ^{64}Cu radiolabeling and immunoPET of human pancreatic adenocarcinoma xenografts (HPAF-II and BxPC-3) (McCabe *et al.*, 2012). In this study, we initially optimized the linker length of the pre-existing ALCAM cDb to maximize diabody formation by reducing the linker length from eight amino acids to five or three amino acids to generate ALCAM-8L, -5L and -3L cDbs, respectively (Fig. 1A). With the validation of diabody formation, we analyzed the targeting capabilities of a site-specific versus non-site-specific DOTA-conjugated anti-ALCAM cDb to human LS174T colorectal carcinoma xenografts not only to monitor the effect of conjugation methodology but also to validate anti-ALCAM as a robust pan-cancer immunoPET agent.

Experimental procedures

Cell lines and media

The human colon carcinoma cell line LS174T (ATCC #CL-188) was maintained in minimum essential medium (Mediatech, Inc.) supplemented with 10% FetalPlex (Gemini Bio-Products), 1% L-glutamine, 1% non-essential amino acids and 1% sodium pyruvate. The rat glioma cell line C6 (ATCC #CCL-107) was maintained in deficient Dulbecco's modification of eagle's basal medium (DMEM) and high glucose (IrvineScientific) supplemented with 10% FetalPlex and 1% L-glutamine. NS0 mouse myeloma cell line (Sigma) (Galfre and Milstein, 1981) was maintained as described (Olafsen *et al.*, 2007).

Cloning

The linker length of the previously described anti-ALCAM-8L cDb (McCabe *et al.*, 2012) was reduced from eight amino acids (GGGGSGGG) to five (GGGGS) or three (GGS) amino acids by site-directed mutagenesis (Agilent Technologies) following manufacturer's instructions to create the anti-

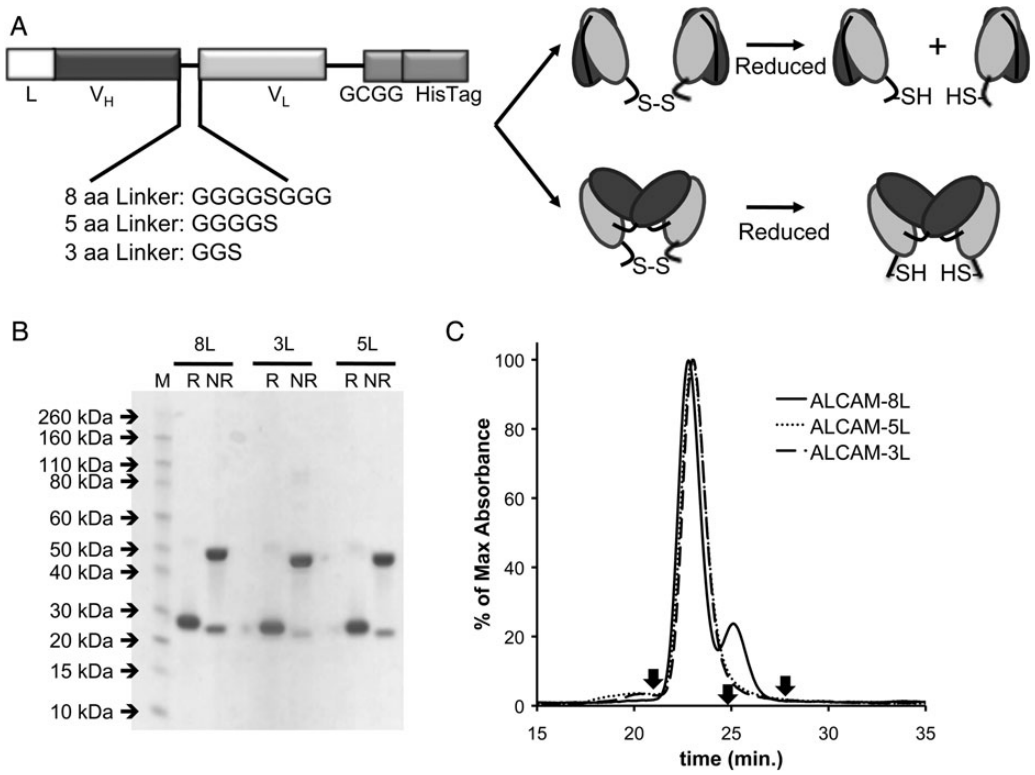

Fig. 1. (**A**) Anti-ALCAM gene assembly displaying linkers of eight, five or three amino acids and schematic representations of the resulting diabody and scFv dimer conformations. L, signal peptide for mammalian cell secretion; V_H, variable heavy domain; V_L, variable heavy domain. (**B**) SDS–PAGE of anti-ALCAM-8L, -5L and -3L cDbs under reducing (R) and non-reducing (NR) conditions. (**C**) Size exclusion chromatography using Superdex 75 column at 0.5 ml/min of anti-ALCAM-8L, -5L, and -3L cDbs using PBS as running buffer. Reference arrows indicate albumin (66 kDa) at 20.8 min, carbonic anhydrase (29 kDa) at 24.7 min, and cytochrome C (12.4 kDa) at 27.4 min.

ALCAM-5L and -3L cDbs, respectively. The following primers were used:

ALCAM-3L-forward: 5′-GTCTCCTCAGGCGGTTCAAATTTTATGCTGACTCAG

ALCAM-3L-reverse: 5′-GCATAAAATTTGAACCGCCTGAGGAGACGGTGACCAG

ALCAM-5L-forward: 5′-GGAGGCGGTTCAAATTTTATGCTGACTCAGGAC

ALCAM-5L-reverse: 5′-CAGCATAAAATTTGAACCGCCTCCACCTGAGGAG

Protein production and purification

Anti-ALCAM-8L, -5L and -3L cDbs were produced and purified as described (McCabe *et al.*, 2012). Briefly, NS0 cells were electroporated with SalI-linearized DNA. Using high dilution, clones were selected using selective glutamine-deficient DMEM (Mediatech, Inc.). Individual clones were screened for cDb production by harvesting supernatants and analyzed by sodium dodecyl sulfate polyacrylamide gel electrophoresis (SDS–PAGE) and western blotting. Blots were probed with alkaline phosphatase-conjugated protein A (Sigma) followed by NBT/BCIP Color Development Substrate kit (Promega).

Alexa Fluor 488 conjugations

Anti-ALCAM-8L, -5L and -3L cDbs were initially conjugated to Alexa Fluor 488 C5-maleimide (mal488; Life Technologies) under reducing conditions. cDbs (~100 μl at 1 mg/ml) were reduced with 10 mM tris[2-carboxyethyl]phosphine hydrochloride (TCEP; Pierce) for 2 h at room temperature. Subsequently, 200 mM of mal488 in DMSO was added directly to the reduced cDb for 2 h at room temperature. Excess dye was removed using a dye removal kit following manufacturer's instructions (Thermo Scientific). Conjugation efficiency was evaluated using the NanoDrop (Thermo Scientific) to calculate the ratio of moles Alexa488 to moles protein. Conjugation efficiency was also measured qualitatively by size exclusion chromatography using a Superdex 75 column (GE Healthcare) on an AKTA purifier (GE Healthcare) and SDS–PAGE-Coomassie stain analysis. Conjugation recovery is defined as the percentage of protein recovered post-conjugation.

DOTA conjugations

For DOTA conjugations, all solutions were made metal-free (MF) using Chelex 100 (1.2 g/l; BioRad). Anti-ALCAM-8L, -5L and -3L cDbs at 1 mg/ml were dialyzed overnight in MF-PBS using Slide-A-Lyzer MINI dialysis units (Thermo Scientific). Non-site-specific conjugation to anti-ALCAM-3L cDb was performed using 1,4,7,10-tetraazacyclododecane-1,4,7,10-tetraacetic acid mono (*N*-hydroxysuccinimide ester) (DOTA-NHS; Macrocyclics) to form anti-ALCAM-3L-amide-DOTA-cDb. Briefly, DOTA-NHS in MF-PBS was added at a 100-fold molar excess of ACLAM cDbs and the pH was adjusted to 8–8.5 immediately using 1 μl additions of 1 M MF-NaOH. The conjugation was allowed to proceed for 2 h before excess NHS-DOTA removal (see below). For site-specific conjugation to the ALCAM cDbs using 1,4,7,10-tetraazacyclododecane-1,4,7-tris-acetic acid-10-maleimidoethylacetamide (malDOTA; Macrocyclics), the ALCAM cDbs were reduced using a 10-fold molar excess of TCEP for 30 min at room temperature. Subsequently, a 20-fold molar excess of malDOTA was added directly to the reduced cDb for 2 h at room temperature. Excess NHS-DOTA or malDOTA was removed using PD-10 desalting columns (GE Healthcare) that were pre-equilibrated with MF-PBS. Eluted protein was concentrated with Amicon Ultra centrifugal filters (0.5 ml and 10 kDa MWCO; Millipore) that had been washed twice with MF-PBS. Conjugation efficiency was measured qualitatively by size exclusion chromatography using a Superdex 75 column on an AKTA purifier and SDS–PAGE-Coomassie stain analysis.

Mass spectrometry

The anti-ALCAM-3L cDb, anti-ALCAM-3L-amide-DOTA-cDb and anti-ALCAM-3L-thioether-DOTA-cDb liquid chromatography–mass spectrometry were acquired and analyzed at City of Hope. Briefly, mass measurements were determined by QToF mass spectrometry using an Agilent 6520, and Agilent nanoflow 1200 HPLC, and a Chip Cube interface with a C8 HPLC chip. Data analysis was performed using Agilent Mass Hunter Bioconfirm software.

MicroPET imaging and analysis

All animal studies were performed under an approved UCLA Chancellor's Animal Research Committee protocol. $3–4 \times 10^6$ cells (LS174T or C6) were harvested and resuspended in 50 μl of DMEM and mixed with 50 μl of Matrigel (BD Biosciences). Cells were implanted subcutaneously in the right (LS174T) and left (C6) shoulder areas of female nude mice (Charles River Laboratories International, Inc.) 9 days prior to microPET imaging. Both ^{64}Cu-DOTA(amide)-cDb and ^{64}Cu-DOTA(thioether)-cDb injected doses contained ~98 μCi cDb (11.6 μg; 8.6 μCi/μg or 0.32 MBq/μg). Doses were prepared in a total volume of 200 μl and were injected via the tail vein. Mice were anesthetized at 4 h post-injection using 2% isoflurane, and 10-min static scans were acquired with an Inveon microPET (Siemens). Filtered back-projection was used for microPET image reconstruction and image analysis was performed using A Medical Imaging Data Examiner (AMIDE) (Loening and Gambhir, 2003).

Biodistribution

Mice were sacrificed after imaging, and tumors and organs were collected and weighed. Tissue activity was measured using a Wizard 3′ 1480 Automatic Gamma Counter (Perkin-Elmer), and decay-corrected values were used to calculate percent injected dose per gram (%ID/g). *T*-tests were performed to determine statistical significance.

Immunohistochemistry

LS174T and C6 tumors were harvested 2 weeks post-implantation for immunohistochemistry (IHC) analysis. Tumors were fixed in 4% formaldehyde overnight, paraffin-embedded and cut into 4 μm sections. Sections were stained for ALCAM as described previously (McCabe *et al.*, 2012).

Results

The anti-ALCAM-8L cDb was initially produced, purified and conjugated to mal488 and malDOTA (Figs. 1–3). Upon SE analysis, however, it was apparent that the anti-ALCAM-8L cDb (Figs. 1C, 2B, 3B solid lines) was produced as a covalent dimer of scFvs and not a diabody. Due to this, site-specific mutagenesis was performed to reduce the linker length from eight to five or three amino acids, creating anti-ALCAM-5L and -3L cDbs respectively, to aid in inter-scFv pairing and

diabody formation (Fig. 1A). All three constructs were produced and purified from NS0 supernatant using ProteinA affinity chromatography to >95% purity as detected by SDS–PAGE under reducing and non-reducing conditions (Fig. 1B). Under non-reducing conditions, the covalent cDbs run as 50 kDa dimers in the presence of denaturing SDS and as 25 kDa monomers upon reduction. SEC analysis showed the three anti-ALCAM constructs eluted at a correct size of ~50 kDa and only anti-ALCAM-8L cDb shows a second peak in the SEC analysis of smaller molecular weight ~25 kDa (Fig. 1C). Recoveries of the anti-ALCAM-8L, -5L and -3L cDbs ranged from 4 to 6.5 mg/l.

After conjugation to mal488, the anti-ALCAM-8L, -5L and -3L cDbs had conjugation recoveries of ~40% and the dye-to-protein molar ratios were 0.9, 1.1 and 1.8, respectively. The anti-ALCAM-8L, -5L and -3L cDbs were analyzed by SDS–PAGE for the detection of protein by Coomassie staining and Alexa Fluor 488 by fluorescence detection (Fig. 2A). The anti-ALCAM-8L, -5L and -3L cDbs all showed protein and fluorescence signal at ~25 kDa in the gel, as expected for a maleimide-conjugated cDb under denaturing SDS conditions (Fig. 2A). In SEC analysis using 280 nm for protein detection and 488 nm for fluorescence detection, it is apparent that both the 5L and 3L remained completely as ~50 kDa diabodies (Fig. 2B) even though they run as ~25 kDa in SDS–PAGE analysis. The 8L cDb, however, elutes as two peaks in both 280 and 488 nm detection at ~50 and ~25 kDa (Fig. 2C), indicating that some species behave as diabodies (51% by 280 nm and 26% by 488 nm absorbance) and some as scFv dimers (49% by 280 nm and 74% by 488 nm absorbance).

A similar analysis was performed for conjugating malDOTA to anti-ALCAM-8L, -5L and -3L cDbs (Fig. 3), showing again that the 8L cDb behaves as an scFv following reduction and site-specific conjugation to malDOTA. For this conjugation method, the 8L, 5L and 3L cDbs had conjugation recoveries of ~80%. In contrast to the mal488 conjugation, the anti-ALCAM-8L cDb conjugation to malDOTA resulted in 100% conversion to the scFv as detected by SEC analysis. Elution profiles are summarized in Table I for the anti-ALCAM-8L, -5L and -3L cDbs under non-reducing conditions for unconjugated protein, mal488-conjugated protein and malDOTA-conjugation, as well as unconjugated protein under reducing conditions (SEC profiles not shown), demonstrating that the 8L cDb is produced as an scFv dimer.

As the anti-ACLAM-3L cDb clearly retained its cross-paired diabody conformation following reduction and modification, it was used for all subsequent experiments. In order to compare non-site-specific with site-specific DOTA conjugation, the 3L cDb was conjugated to lysines using NHS-DOTA and to the reduced cysteines using maleimide-DOTA, resulting in ALCAM-3L-amide-DOTA-cDb and ALCAM-3L-thioether-DOTA-cDb, respectively. Mass spectrometry confirmed the addition of one to five DOTAs per diabody for the ALCAM-3L-amide-DOTA-cDb and exactly two DOTAs per diabody for the ALCAM-3L-thioether-DOTA-cDb (Table II).

When radiolabeled with ^{64}Cu, ALCAM-3L-amide-DOTA-cDb and ALCAM-3L-thioether-DOTA-cDb achieved specific activities of 8.6 μCi/μg (0.32 MBq/μg). Importantly, these conjugated ALCAM cDb's retained their ability to bind the ALCAM-expressing colon cancer cell line LS174T as the immunoreactive fraction of both ^{64}Cu-radiolabeled ALCAM cDb's were 83%. Approximately 11.6 μg of cDb was injected into mice bearing ALCAM-positive LS174T tumors and antigen-negative C6 tumors. Four hours post-injection, immunoPET images were acquired (Fig. 4) and biodistributions were performed (Table III). Uptake in the LS174T tumor was 1.4 ± 0.15%ID/g and 2.6 ± 0.53%ID/g for ALCAM-3L-amide-DOTA-cDb and ALCAM-3L-thioether-DOTA-cDb, respectively, and 0.99 ± 0.06%ID/g and 1.4 ± 0.06%ID/g for the antigen-negative C6 tumor. The ALCAM-3L-thioether-DOTA-cDb also had higher blood activity (1.4 ± 0.15%ID/g) than the ALCAM-3L-amide-DOTA-cDb (0.97 ± 0.11%ID/g), indicating a slower blood clearance. The corresponding LS174T tumor-to-blood ratios of the ALCAM-3L-amide-DOTA-cDb and ALCAM-3L-thioether-DOTA-cDb were 1.4 and 1.9, respectively.

Interestingly, the different conjugation strategies altered both the liver and kidney uptakes; ALCAM-3L-amide-DOTA-cDb had kidney and liver uptakes of 51 ± 5.7%ID/g and 36 ± 2.9%ID/g, while the ALCAM-3L-thioether-DOTA-cDb had kidney and liver uptakes of 95 ± 9.5%ID/g and 20 ± 2.5%ID/g. Furthermore, the ALCAM-3L-thioether-DOTA-cDb shows enhanced uptake in the salivary glands and eyes when compared with the ALCAM-3L-amide-DOTA-cDb. PET images

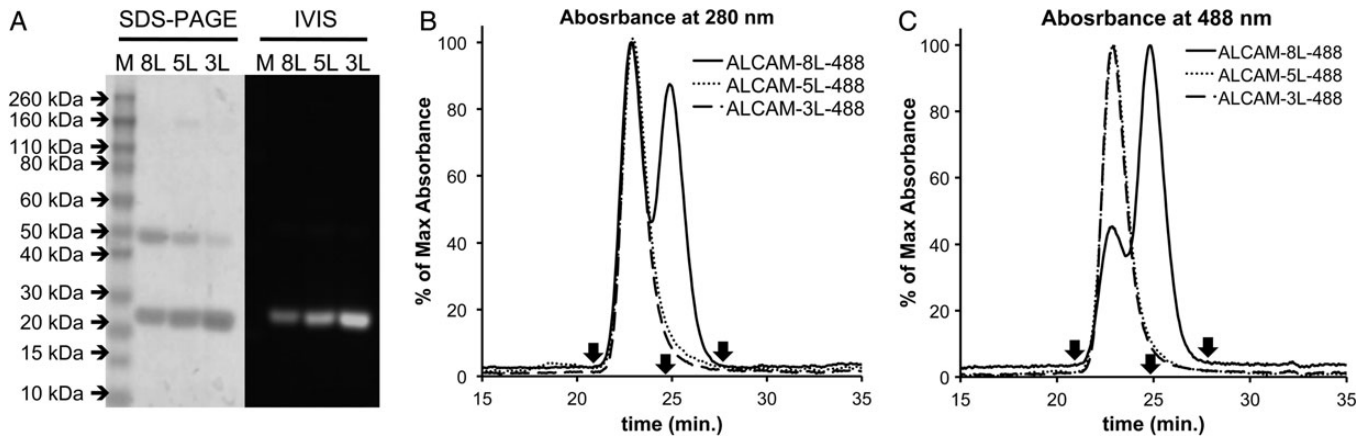

Fig. 2. Analysis of mal488 conjugation to anti-ALCAM-8L, -5L, and -3L cDbs. (**A**) SDS–PAGE of anti-ALCAM-8L, -5L, and -3L cDbs post-mal488 conjugation shown as Coomassie stain (left panel) and fluorescence (right panel). Size exclusion chromatography analysis at 280 nm (**B**) and 488 nm (**C**) using Superdex 75 column at 0.5 ml/min of mal488-conjugated anti-ALCAM-8L, -5L and -3L cDbs using PBS as running buffer. Reference arrows indicate albumin (66 kDa) at 20.8 min, carbonic anhydrase (29 kDa) at 24.7 min, and cytochrome C (12.4 kDa) at 27.4 min.

shown at different scales clearly represent the difference in uptake in the kidneys, liver, salivary glands, eyes and tumors of the site-specific versus non-site-specific DOTA-conjugation methods (Fig. 4). IHC was performed on both LS174T and C6 xenografts for ALCAM expression, indicating that the LS174T xenografts do express ALCAM in this model (Fig. 5). As shown here, conjugation strategy greatly affects the pharmacokinetics of cDb fragments and the site-specific conjugation strategy of the ALCAM cDb allows for increased tumor uptake and higher tumor-to-blood ratios than non-site-specifically conjugated cDb.

Discussion

Anti-ALCAM cDbs with linker lengths of eight, five and three amino acids were engineered, expressed at high levels in mammalian culture and efficiently purified by affinity chromatography. With extensive analysis using SDS–PAGE and SEC of native and site-specifically conjugated anti-ALCAM-8L, -5L and -3L cDbs to mal488 and malDOTA, it was determined that the 8L construct is a dimer of scFvs and not a true cDb. For the mal488 conjugations, the conjugation efficiencies varied from 0.9 to 1.8 fluorescent molecules per protein and the protein recoveries were very low. This conjugation method was not optimized further due to the low recovery but it did allow us to monitor the effect of conjugation to the engineered cysteine by the fluorescent Alexa Fluor 488. On the other hand, the malDOTA conjugations had recoveries of ~80% and this could be due to the difference in hydrophobicity of the Alexa Fluor 488 and the DOTA chelator.

It has been shown that linker lengths of ≤12 aa cause an scFv to form Dbs (Whitlow *et al.*, 1994; Kortt *et al.*, 1997) and other examples of diabody construction using linker lengths as long or longer than the anti-ALCAM-8L cDb described in this work exist, for example anti-neuraminidase (10 aa (Kortt *et al.*, 1997)), anti-CEA (8 aa (Wu *et al.*, 1999)) and anti-CD20 (8 aa (Olafsen *et al.*, 2010)). Furthermore, shorter linker lengths can cause multimerization into trimeric and/or tetrameric species (Kortt *et al.*, 1997; Kelly *et al.*, 2008). In this study, SEC showed a linker length of three amino acids did not induce multimerization. Individual pairs of V_H and V_L domains from different scFvs seem to behave differently in their ability to consistently form Dbs, and this could be due to V domain-interface stability, V domain stability and V domain orientation. Combined with reports that linkers of 18 aa can cause multimerization of certain scFv constructs (Whitlow *et al.*, 1994; Le Gall *et al.*, 1999), the work described here demonstrates the importance of rigorous characterization when constructing cDbs.

With the validation of true diabody conformation, we conjugated the ALCAM-3L cDb to the ^{64}Cu chelator DOTA either site specifically via the engineered cysteines or non-site specifically via solvent-exposed lysines using maleimide-DOTA or NHS-DOTA, respectively. Mass spectrometry confirmed the conjugation strategy of exactly two DOTA conjugations per ALCAM-3L-thioether-DOTA-cDb and a distribution of one to five DOTA conjugations per ALCAM-3L-amide-DOTA-cDb. The ALCAM-3L-thioether-DOTA-cDb mass spectrometry showed a single peak consistent with the expected mass change from conjugation. The site-specific conjugation has allowed for the production of a single, chemically defined product for imaging that is still able to be radiolabeled with ^{64}Cu and retains the ability to bind to ALCAM.

Upon ^{64}Cu radiolabeling, the immuno-reactive fraction of both ALCAM-3L-thioether-DOTA-cDb and ALCAM-3L-amide-DOTA-cDb was very similar (~83%), indicating that one to five DOTA conjugation per ALCAM-3L-amide-DOTA-cDb does not disrupt antigen binding. In xenograft models of C6 and LS174T tumors in nude mice, targeting of the ALCAM-positive LS174T xenograft was enhanced for the site-specific ALCAM-3L-thioether-DOTA-cDb even though both probes had similar immuno-reactivities. Enhanced tumor targeting could be due to the increased blood activity of the ^{64}Cu-ALCAM-3L-thioether-DOTA-cDb compared with the ^{64}Cu-ALCAM-3L-amide-DOTA-cDb, as indicated by their blood %ID/g at 4 h post-injection (1.4 ± 0.15 and 0.97 ± 0.11%ID/g, respectively).

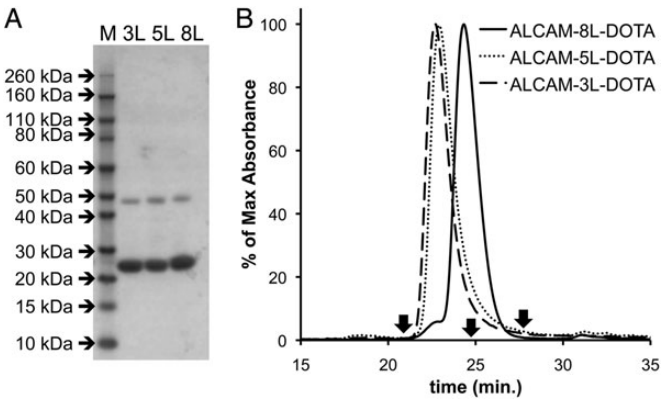

Fig. 3. Analysis of malDOTA conjugation to anti-ALCAM-8L, -5L and -3L cDbs. (**A**) SDS–PAGE of anti-ALCAM-8L, -5L and -3L cDbs post-malDOTA conjugation. (**B**) Size exclusion chromatography analysis at 280 nm using the Superdex 75 column at 0.5 ml/min of malDOTA-conjugated anti-ALCAM-8L, -5L, and -3L cDbs using PBS as a running buffer. Reference arrows indicate albumin (66 kDa) at 20.8 min, carbonic anhydrase (29 kDa) at 24.7 min and cytochrome C (12.4 kDa) at 27.4 min.

Table I. Elution times of unconjugated anti-ALCAM-8L, 5L, and 3L cDbs in non-reducing conditions and reducing conditions, and mal488- and malDOTA-conjugated anti-ALCAM-8L, 5L and 3L cDbs in non-reducing conditions using Superdex 75 size exclusion chromatography. Elution times are shown in minutes and numbers in parentheses indicate the percentage at each retention time if applicable. Note the reference elution times are as follows: albumin (66 kDa) at 20.8 min, carbonic anhydrase (29 kDa) at 24.7 min and cytochrome C (12.4 kDa) at 27.4 min

	Non-reducing		Reducing		Maleimide-488		Maleimide-DOTA	
Construct	cDb	scFv	cDb	scFv	cDb	scFv	cDb	scFv
ALCAM-8L	22.80 (82%)	25.10 (18%)	n/a	24.95	22.85 (51%)	24.80 (49%)	n/a	24.32
ALCAM-5L	22.98	n/a	23.31	n/a	22.91	n/a	22.86	n/a
ALCAM-3L	23.02	n/a	23.11	n/a	22.85	n/a	22.70	n/a

Increased blood activity enables greater tumor exposure, resulting in enhanced ALCAM-positive LS174T targeting of the ^{64}Cu-ALCAM-3L-thioether-DOTA-cDb. Importantly, the ^{64}Cu-ALCAM-3L-thioether-DOTA-cDb has higher LS174T tumor-to-blood ratios when compared with the ^{64}Cu-ALCAM-3L-amide-DOTA-cDb even though the blood activity is higher. Altered serum half-life could be due to a variety of factors, including change in the overall surface charge due to conjugation strategy, increased flexibility of the ALCAM-3L-thioether-

Table II. Mass spectrometry review of intact unconjugated anti-ALCAM-3L cDb, anti-ALCAM-3L-amide-DOTA-cDb and anti-ALCAM-3L-thioether-DOTA-cDb. Expected addition of one amide-DOTA conjugation is 386.2 kDa and one thioether-DOTA is 526.2 kDa

	Modification	Expected (kDa)	Found (kDa)	Difference (kDa)
Unconjugated	n/a	50344.2	50341.6	−2.6
NHS-DOTA	0× DOTA	50344.2	50342.3	−1.9
	1× DOTA	50730.4	50729.3	−1.1
	2× DOTA	51116.8	51115.2	−1.4
	3× DOTA	51502.8	51501.3	−1.5
	4× DOTA	51889.0	51888.1	−0.9
	5× DOTA	52275.2	52275.5	+0.3
malDOTA	0× DOTA	25173.1	25138.2	−34.9
	1× DOTA	25699.3	25716.8	+17.5

Table III. Biodistribution of ^{64}Cu-ALCAM-3L-amide-DOTA-cDb and ^{64}Cu-ALCAM-3L-thioether-DOTA-cDb at 4 h post-injection of female nude mice bearing ALCAM-positive LS174T and ALCAM-negative C6 xenografts

	% ID/g ± SD		
Organ	amide-DOTA ($n = 4$)	Thioether-DOTA ($n = 4$)	P
Blood	0.97 ± 0.11	1.4 ± 0.15	<0.01
LS174T (+)	1.4 ± 0.15	2.6 ± 0.53*	<0.01
C6 (−)	0.99 ± 0.06	1.4 ± 0.06	<0.0001
Spleen	3.8 ± 0.38	2.6 ± 0.19	<0.005
Stomach	1.5 ± 0.27	4.0 ± 0.29	<0.0001
Intestines	2.0 ± 0.16	4.3 ± 0.04	<0.0001
Liver	36 ± 2.9	20. ± 2.5	<0.0005
Kidneys	51 ± 5.7	95 ± 9.5	<0.0005
Heart	1.2 ± 0.11	1.4 ± 0.09	<0.05
Lungs	2.2 ± 0.20	3.7 ± 0.35	<0.0005
Muscle	0.19 ± 0.02	0.24 ± 0.03	0.054
Carcass	0.61 ± 0.04	0.78 ± 0.03	<0.0005

*$n = 3$, P-values for LS174T versus C6 for amide-DOTA and thioether-DOTA are <0.005 and <0.01, respectively.

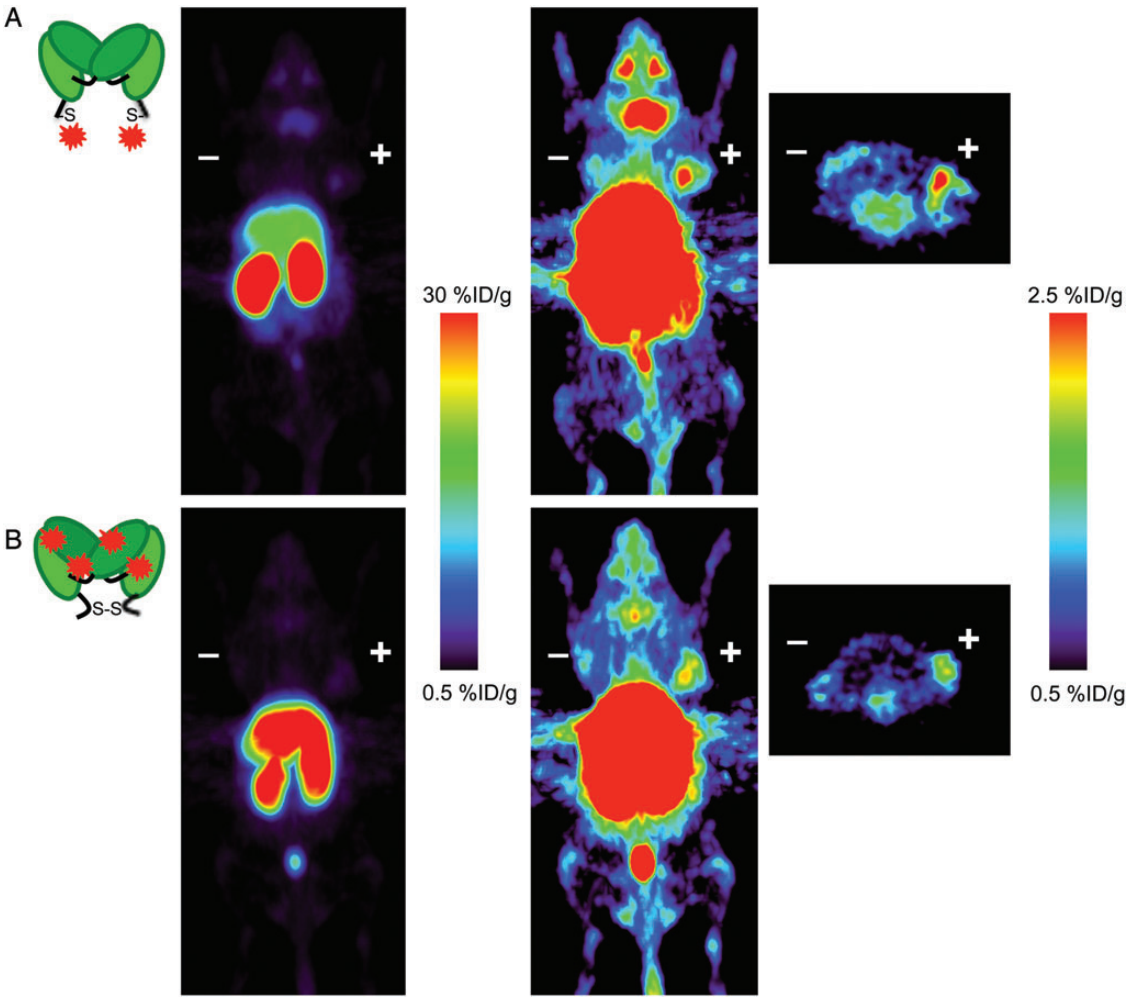

Fig. 4. ImmunoPET images in athymic nude mice bearing ALCAM-positive LS174 T (right) and ALCAM-negative C6 (left) tumors acquired 4 h post-injection shown at different thresholds for comparing both tumor targeting and non-tumor biodistribution of the ^{64}Cu-ALCAM-3L-amide-DOTA-cDb (**A**) and ^{64}Cu-ALCAM-3L-thioether-DOTA-cDb (**B**). Coronal PET images are shown as 25 mm maximum intensity projections and transverse PET images are 2 mm maximum intensity projections.

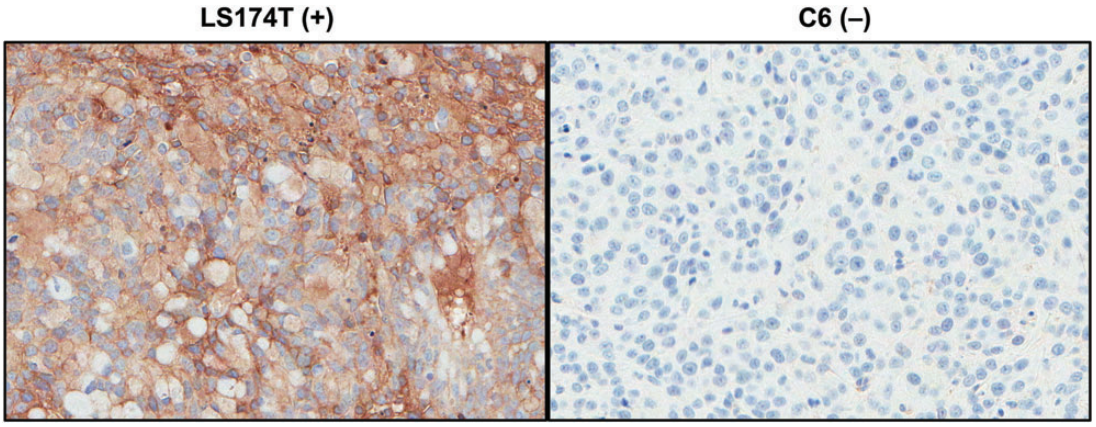

Fig. 5. *Ex vivo* IHC of ALCAM-positive LS174T (left) and ALCAM-negative C6 (right) xenografts stained for ALCAM expression.

DOTA-cDb compared with the ALCAM-3L-amide-DOTA-cDb due to conjugation of the engineered thiol, and the effects of the proximity of two hexahistidine tags of the ALCAM-3L-amide-DOTA-cDb when the engineered thiols form a disulfide bond.

The internalization of this anti-ALCAM cDb construct (Liu *et al.*, 2004) requires the use of residualizing PET radionuclides for retention of activity in target tissues. An offshoot is that organs of clearance (i.e. liver and kidney) also retain residualizing activity. High uptake in the kidneys, as seen here, is expected because the cDbs are below the renal filtration cutoff (Vegt *et al.*, 2010). However, liver uptake is high when compared with other residualizing radioisotope-labeled Dbs (Yazaki *et al.*, 2001; Schneider *et al.*, 2009). This is most likely due to transchelation of ^{64}Cu from DOTA to enzymes in the liver (Anderson and Ferdani, 2009). Interestingly, the resulting pharmacokinetic profiles of the two ^{64}Cu-radiolabeled probes showed altered kidney and liver uptakes, as well as altered blood activity as mentioned above. The ^{64}Cu-ALCAM-3L-amide-DOTA-cDb exhibited higher liver and lower kidney uptake when compared with the ^{64}Cu-ALCAM-3L-thioether-DOTA-cDb. This could be due to the same reasons for altered blood clearance: surface charge, flexibility and histidine tags. As kidneys are radiosensitive, methods exist to reduce the renal radioactivity levels of the ^{64}Cu-ALCAM-3L-amide-DOTA-cDb (Arano, 1998). Not only do the kidney and liver uptakes vary, but immunoPET clearly shows enhanced uptake of ^{64}Cu-ALCAM-3L-thioether-DOTA-cDb to the salivary glands and eyes. This anti-ALCAM construct is cross-reactive with mouse and human ALCAM (McCabe *et al.*, 2012), and salivary glands and retinal endothelium are known to express ALCAM (Abidi *et al.*, 2006; Smith *et al.*, 2012). The utilization of ALCAM knockout mice could validate whether salivary gland and retinal targeting of the ^{64}Cu-ALCAM-3L-thioether-DOTA-cDb is target specific.

The concept of altered pharmacokinetics for differing radiolabeling methods based on radioisotope, chelator and conjugation strategy has not been analyzed rigorously for antibody fragments. Previously, peptide linkers have been shown to alter the kidney uptake of DOTA-conjugated anti-CEA cDb (Li *et al.*, 2002). However, many studies have been performed with affibodies that highlight the importance of His-tag sequence, location of His-tag, chelator, radiometal and method of conjugation (Tolmachev and Orlova, 2010; Hofstrom *et al.*, 2013; Strand *et al.*, 2013). These studies highlight the potential effects that radiolabeling strategy can have on diabody tumor targeting and pharmacokinetics.

In conclusion, both conjugation strategies allowed for the targeting and imaging of ALCAM-positive LS174T xenografts *in vivo*. Interestingly, even though the non-site-specific conjugation did not affect the immunoreactivity of the radiolabeled cDb when compared with the site-specific conjugation, the site-specific ALCAM-3L-thioether-DOTA-cDb variant exhibited enhanced tumor-to-blood and positive-to-negative tumor ratios when compared with the ALCAM-3L-amide-DOTA-cDb. Furthermore, the nature of the conjugation had a drastic impact on renal and hepatic uptake and needs to be considered when developing immunoPET agents. The altered tumor targeting and pharmacokinetic profile could be due to the change in surface charge of the diabody post-DOTA-conjugation and the change in physical structure that results from the reduction and subsequent conjugation to the engineered cysteine residue of the site-specific ALCAM-3L-thioether-DOTA-cDb conjugate. Successful immunoPET imaging of ALCAM expression in both pancreatic (McCabe *et al.*, 2012) and colon cancers suggests further investigation of ALCAM as a pan-cancer imaging biomarker.

Acknowledgements

The authors would like to thank Waldemar Ladno, Darin Williams and Dr. David Stout at the Crump Institute for Molecular Imaging at UCLA for their help with the PET scans and both Roger Moore and Bogdan Gugiu at City of Hope for Mass Spectrometry analysis. Furthermore, the authors thank the Genoseq Core Facility at UCLA and the Jonsson Comprehensive Cancer Center.

Conflict of interest: A.M.W. is a founder and consultant to ImaginAb, Inc. and J.D.M. is a consultant to ImaginAb, Inc.

Funding

This work was supported by the National Institutes of Health Scholars in Oncological Medical Imaging training program at UCLA [R25T CA098010]. Imaging studies were funded in part by the Cancer Center Support Grant [NIH P30 CA016042].

References

Abidi,S.M., Saifullah,M.K., Zafiropulos,M.D., Kaput,C., Bowen,M.A., Cotton,C. and Singer,N.G. (2006) *J. Clin. Immunol.*, **26**, 12–21.

Anderson,C.J. and Ferdani,R. (2009) *Cancer Biother. Radiopharm.*, **24**, 379–393.
Arano,Y. (1998) *Q. J. Nucl. Med.*, **42**, 262–270.
Barat,B., Sirk,S.J., McCabe,K.E., *et al*. (2009) *Bioconjug. Chem.*, **20**, 1474–1481.
Bowen,M.A., Patel,D.D., Li,X., *et al*. (1995) *J. Exp. Med.*, **181**, 2213–2220.
Camarero,J.A. (2008) *Biopolymers*, **90**, 450–458.
Chen,R., Yi,E.C., Donohoe,S., *et al*. (2005) *Gastroenterology*, **129**, 1187–1197.
Chitteti,B.R., Kobayashi,M., Cheng,Y., *et al*. (2014) *Blood* [Epub ahead of print].
Galfre,G. and Milstein,C. (1981) *Methods Enzymol.*, **73**, 3–46.
Hofstrom,C., Altai,M., Honarvar,H., Strand,J., Malmberg,J., Hosseinimehr,S.J., Orlova,A., Graslund,T. and Tolmachev,V. (2013) *J. Med. Chem.*, **56**, 4966–4974.
Junutula,J.R., Raab,H., Clark,S., *et al*. (2008) *Nat. Biotechnol.*, **26**, 925–932.
Kelly,M.P., Lee,F.T., Tahtis,K., Power,B.E., Smyth,F.E., Brechbiel,M.W., Hudson,P.J. and Scott,A.M. (2008) *Cancer Biother. Radiopharm.*, **23**, 411–423.
King,J.A., Ofori-Acquah,S.F., Stevens,T., Al-Mehdi,A.B., Fodstad,O. and Jiang,W.G. (2004) *Breast Cancer Res.*, **6**, R478–R487.
Knowles,S.M. and Wu,A.M. (2012) *J Clin Oncol*, **30**, 3884–3892.
Kortt,A.A., Lah,M., Oddie,G.W., *et al*. (1997) *Protein Eng.*, **10**, 423–433.
Kristiansen,G., Pilarsky,C., Wissmann,C., *et al*. (2005) *J. Pathol.*, **205**, 359–376.
Le Gall,F., Kipriyanov,S.M., Moldenhauer,G. and Little,M. (1999) *FEBS Lett.*, **453**, 164–168.
Li,L., Olafsen,T., Anderson,A.L., Wu,A., Raubitschek,A.A. and Shively,J.E. (2002) *Bioconjug. Chem.*, **13**, 985–995.
Liu,B., Conrad,F., Cooperberg,M.R., Kirpotin,D.B. and Marks,J.D. (2004) *Cancer Res.*, **64**, 704–710.
Liu,B., Conrad,F., Roth,A., Drummond,D.C., Simko,J.P. and Marks,J.D. (2007) *J. Mol. Med. (Berl)*, **85**, 1113–1123.
Liu,C.C. and Schultz,P.G. (2010) *Annu. Rev. Biochem.*, **79**, 413–444.
Loening,A.M. and Gambhir,S.S. (2003) *Mol. Imaging*, **2**, 131–137.
McCabe,K.E., Liu,B., Marks,J.D., Tomlinson,J.S., Wu,H. and Wu,A.M. (2012) *Mol. Imaging Biol.*, **14**, 336–347.
Mezzanzanica,D., Fabbi,M., Bagnoli,M., *et al*. (2008) *Clin. Cancer Res.*, **14**, 1726–1733.
Ofori-Acquah,S.F. and King,J.A. (2008) *Transl. Res.*, **151**, 122–128.
Olafsen,T., Cheung,C.W., Yazaki,P.J., *et al*. (2004) *Protein Eng. Des. Sel.*, **17**, 21–27.
Olafsen,T., Gu,Z., Sherman,M.A., *et al*. (2007) *J. Immunother.*, **30**, 396–405.
Olafsen,T., Sirk,S.J., Betting,D.J., Kenanova,V.E., Bauer,K.B., Ladno,W., Raubitschek,A.A., Timmerman,J.M. and Wu,A.M. (2010) *Protein Eng. Des. Sel.*, **23**, 243–249.
Patel,D.D., Wee,S.F., Whichard,L.P., Bowen,M.A., Pesando,J.M., Aruffo,A. and Haynes,B.F. (1995) *J. Exp. Med.*, **181**, 1563–1568.
Schliemann,C., Roesli,C., Kamada,H., Borgia,B., Fugmann,T., Klapper,W. and Neri,D. (2010) *Blood*, **115**, 736–744.
Schneider,D.W., Heitner,T., Alicke,B., *et al*. (2009) *J. Nucl. Med.*, **50**, 435–443.
Sirk,S.J., Olafsen,T., Barat,B., Bauer,K.B. and Wu,A.M. (2008) *Bioconjug. Chem.*, **19**, 2527–2534.
Sletten,E.M. and Bertozzi,C.R. (2009) *Angew. Chem. Int. Ed. Engl.*, **48**, 6974–6998.
Smith,J.R., Chipps,T.J., Ilias,H., Pan,Y. and Appukuttan,B. (2012) *Exp. Eye Res.*, **104**, 89–93.
Strand,J., Honarvar,H., Perols,A., Orlova,A., Selvaraju,R.K., Karlstrom,A.E. and Tolmachev,V. (2013) *PloS ONE*, **8**, e70028.
Strassberger,V., Gutbrodt,K.L., Krall,N., Roesli,C., Takizawa,H., Manz,M.G., Fugmann,T. and Neri,D. (2014) *J. Proteomic.*, **99**, 138–151.
Swart,G.W., Lunter,P.C., Kilsdonk,J.W. and Kempen,L.C. (2005) *Cancer Metastasis Rev.*, **24**, 223–236.
Tait,J.F., Smith,C., Levashova,Z., Patel,B., Blankenberg,F.G. and Vanderheyden,J.L. (2006) *J. Nucl. Med.*, **47**, 1546–1553.
Tavaré,R., Torres Martin De Rosales,R., Blower,P.J. and Mullen,G.E. (2009) *Bioconjug. Chem.*, **20**, 2071–2081.
Tolmachev,V. and Orlova,A. (2010) *Curr. Med. Chem.*, **17**, 2636–2655.
van Kempen,L.C., van den Oord,J.J., van Muijen,G.N., Weidle,U.H., Bloemers,H.P. and Swart,G.W. (2000) *Am. J. Pathol.*, **156**, 769–774.
Vegt,E., de Jong,M., Wetzels,J.F.M., Masereeuw,R., Melis,M., Oyen,W.J.G., Gotthardt,M. and Boerman,O.C. (2010) *J. Nucl. Med.*, **51**, 1049–1058.
Weichert,W., Knosel,T., Bellach,J., Dietel,M. and Kristiansen,G. (2004) *J. Clin. Pathol.*, **57**, 1160–1164.
Whitlow,M., Filpula,D., Rollence,M.L., Feng,S.L. and Wood,J.F. (1994) *Protein Eng.*, **7**, 1017–1026.
Wiiger,M.T., Gehrken,H.B., Fodstad,O., Maelandsmo,G.M. and Andersson,Y. (2010) *Cancer Immunol. Immunother.*, **59**, 1665–1674.
Wu,A.M. (2009) *J. Nucl. Med.*, **50**, 2–5.
Wu,A.M. (2014) *Methods*, **65**, 139–147.
Wu,A.M. and Senter,P.D. (2005) *Nat. Biotechnol.*, **23**, 1137–1146.
Wu,A.M., Williams,L.E., Zieran,L., *et al*. (1999) *Tumor Target*, **4**, 47–58.
Yazaki,P.J., Wu,A.M., Tsai,S.W., Williams,L.E., Ikle,D.N., Wong,J.Y.C., Shively,J.E. and Raubitschek,A.A. (2001) *Bioconjug. Chem.*, **12**, 220–228.